Enhancement in Corrosion Resistance and Hardness of AZ91D Magnesium Alloy by Carbon Ion Implantation

M. Kashif Mumtaz[1], G. Murtaza[1*]

[1] Centre for Advanced Studies in Physics, GC University, Lahore-54000

ARTICLE INFO

ABSTRACT

To improve the mechanical and corrosion resistance of AZ91D magnesium alloy, carbon ion implantation technique has been carried out using 2 MV Pelletron accelerator on the polished magnesium alloy surface. Vickers hardness test, particle induced X-ray emission (PIXE) analysis, scanning electron microscopy (SEM), X-ray diffraction (XRD) and corrosion tests are employed to analyse the properties. Vickers hardness tests revealed the improvement in surface hardness which we infer is due to the enhancement in dislocation density, as a consequence of carbon ion implantation with varied dose from 1.26×10^{13} to 8.4×10^{14} ions-cm^{-2}. That is, the increase in hardness is directly related to the ion dose, variation in lattice parameters, crystallite size, and change in peak intensity, all due to the increase in ion fluence. The non-destructive elemental analysis, PIXE, gave the elemental profile before and after ion implantation. SEM results indicated that singly ionized carbon ion implantation has modified the surface of AZ91D Mg-alloy. XRD results showed that the unexposed and treated samples include α-Mg and β-Mg$_{17}$Al$_{12}$ phases. XRD results also revealed that after the carbon ion implantation the diffraction peak position and intensity of all the phases shifted. The corrosion tests were carried out using two methods, namely, weight loss method and electrochemical test. The results guided that for a higher dose of ion implantation, the corrosion resistance increased and loss of mass of exposed surface of specimens decreased, which reflect the enhancement of corrosion resistance.

Corresponding Author's Email: gmrai@gcu.edu.pk

1.   Introduction

Magnesium has a vast area of applications in pure and alloy form in; automotive, biomedical, electronics and aerospace industry. Despite lighter in weight, it has high specific strength and dimensional stability, and recycling potential (Höche, Blawert, Cavellier, Busardo, & Gloriant, 2011; Ueda, Reuther, & Lepienski, 2005; Wang, Li, Xiong, Tian, & Yang, 2011). Magnesium is the lightest by weight among all commonly used materials with a density of 1.74 g-cm^{-3} which is approximately one-third of that of aluminium. It oxidizes/corrodes in normal humid air, and the oxide layer thus developed does not shield the rest from humidity and further corrosion carries on. This deprived corrosion resistance limits its use in many industrial applications (H. Liu, Xu, Jiang, Wang, & Zhang, 2013; Song, Johannesson, Hapugoda, & StJohn, 2004; Tian, Wei, Yang, Fu, & Chu, 2005). The main reason is its low potential (E_0 = -2.34 V vs. normal hydrogen electrode) even against the normal atmospheric conditions.

The corrosion is defined as the eating away of metals and alloys due to physical, chemical and electrochemical reactions with its environment. It depends upon the movement of the electrons, ions and atoms (R. Xu et al., 2012). Increase in corrosion resistance may cause a decrease in corrosion rate which will not only enhance the mechanical properties but also a life of parts in automation, communication and consumer electronics, aerospace engineering, electromagnetic shielding and good dimensional stability.

Generally, corrosion is classified into two types. (a) Aqueous or wet corrosion. (b) Dry corrosion due to interaction between metal and any oxidizing gas like oxygen, carbon dioxide or oxidizing sulphur at elevated temperatures (Suresh, Srinivasan, Pillai, & Pai, 2013). Wet corrosion is produced in the prances of liquid (water) or an aqueous solution of electrolytes. Dry corrosion is produced in the absence of a liquid phase. In this kind of corrosion, vapours and gases are the co rodents at high temperatures (Y. Li et al., 2014). Several workers have explored different techniques for the surface modifications of Mg alloys; physical vapour deposition, nitrogen ion implantation, chemical conversion coatings, micro-arc oxidation, electroless nickel deposition, ion implantation, super-hydrophobic coating, chemical conversion coating and slippery coatings (Butt et al., 2019; Gu, Yan, Zhang, & Tu, 2016; Y. Li et al., 2014; Suresh et al., 2013; Tian et al., 2005; R. Xu et al., 2012; J. Zhang, Gu, Tong, Yan, & Tu, 2016; J. Zhang, Gu, & Tu, 2017).

Ion implantation is a material modification process in which ions are accelerated and bombarded on the surface of the sample. In this material-engineering process, the mechanical, electrical, chemical and physical properties of materials are modified. Mostly, it is used for the fabrication of semiconductor devices, and for metal finishing and various applications of material science projects (Tian et al., 2005). If the implanted ions have a mass comparable to the atoms of the target surface, then atoms of the sample are knocked out resulting in local surface modification. Ion implantation, especially, carbon ion implantation, has given significant results to enhance the corrosion resistance (Höche et al., 2011; H. Liu et al., 2013; Ueda et al., 2005; Wang et al., 2011) and/or mechanical properties (Butt et al., 2019; Y. Li et al., 2014; H. Liu et al., 2013; Song et al., 2004; Suresh et al., 2013; Tian et al., 2005; R. Xu et al., 2012). For biomedical applications, the corrosion resistance of magnesium alloys must be improved while maintaining the surface morphology and biocompatibility. For this purpose, carbon has beneficial, clinical, chemical, and physical characteristics (Höche et al., 2011; H. Liu et al., 2013; Ueda et al., 2005; Wang et al., 2011). Therefore, carbon ion implantation technique may help to enhance the corrosion resistance and biocompatible characteristics of Mg-alloy. Carbon ion implantation may increase the electrochemical behaviour of Mg-alloy, demonstrating remarkable improvement in corrosion resistance. Previously, carbon ion implantations gave reasonably good results on steel, aluminium, titanium and zirconium alloys. Having knowledge of the known possibilities, based on prior work by several authors (Butt et al., 2019). In this study, carbon ion implantation on AZ91D magnesium alloy is studied and the consequent improvement in corrosion resistance and the changes of mechanical properties have been calculated.

2.   Experimental Details
2.1. Sample Preparations

Total eight number of AZ91D Mg alloy samples, with a thickness of 0.5 cm (each) were prepared. Whereas, four were cut into a square [2×2 cm^2] and the other four were rectangular strips [4×2 cm^2]. After cutting, the samples were ground up employing abrasive SiC papers, sequentially with 320, 500, 1000, 1500, 2000 and 3000 grits, followed by final polishing using 10 μm diamond paste. After each stage of grinding and final polishing, the samples were carefully washed using an ultrasonic bath and rinsed with acetone.
Note that out of eight samples, one pair (one squared and one rectangular shaped) were kept without ion implantation (we name these as untreated) and other three pair were dosed with similar three ion implantations and are named as sample1, sample2 and sample3 respectively. One set of four samples (squared ones) were used for XRD, SEM and PIXE analyses, whereas the other set was used for micro hardness and electrochemical tests.

2.2. Ion Implantation and Characterizations

Three pair of AZ91D Mg-alloy were selected for ion implantation. Singly charged carbon ions were used for implantation in evacuated target chamber of 2 MV Pelletron accelerator, installed at CASP, GC University Lahore. These ions were produced by sputtering from cesium target. A maximum of 500 keV energy was given to the carbon ions, which is enough to make the ions stay near the surface of the sample (Höche et al., 2011). Energy remained the same for all three pair but dose (ions-cm^{-2}) was different which is: 1.26×10^{13}, 5.0×10^{13} and 8.4×10^{14}.

PIXE analysis of the untreated and carbon-beam treated samples were carried out, setting the beam of protons to an energy of 4 MeV and maintaining a current of 20 nA as optimized set of parameters (Shafique et al., 2016), giving good combination of background ratios and high cross-section for the element of interest (AZ91D in our case). The diameter of the beam was adjusted to 400 μm and samples were placed perpendicularly facing the beam. A Si-Li detector was placed at an orientation of 45° to the beam direction and 10 cm apart from the sample. The consequent characteristic x-ray spectra were collected at the detector of a multi-channel analyser and were concluded using GUPIX software.

2.3. Corrosion Tests
2.3.1. Weight Loss Method

Weight loss method is the most commonly used technique of all corrosion rate measurements (Yan et al., 2015). The samples were measured for weight and then exposed to a corrodent for a known period followed by re-weight. The rate of loss in mass due to corrosion can be calculated by using

$$R = KW/\rho AT \tag{1}$$
$$W = R\rho AT/K \tag{2}$$

Where W is weight loss (gm), R is corrosion rate (mmpy), ρ is density (g cm^{-3}), A is the area (cm^2), T is a time of exposure (hours or days) and K is constant. Weight loss is measured in mg dm^{-3} (days). It is time dependent technique in which time duration of (2, 10, 15, 20 and 30 days) was used. The corrosion rate is expressed in mills penetration per year (mpy). The corrosion rate in (mpy) can be calculated by using, mpy = $534 W/DAT$. Where W = weight loss in mg, A = Area in sq. cm, T = time of exposure in hours, D is the density of the metal in g cm^{-3} (Khosro Aghayani & Niroumand, 2011; P. Li, Han, Xin, Zhu, & Lei, 2008).

2.3.2. Electrochemical Test

The corrosion rate of the metals/alloys can be calculated in a more rigorous way of using the electrochemical test, based on Faraday's first law, as described in theory, the current is uniformly distributed over the wetted surface area (Baboian, 2005).

$$CR(mmpy) = \frac{K_1 i_{corr}(E.W.)}{\rho} \tag{3}$$

Where CR is the corrosion rate (mmpy), K_1 is constant (3.27×10^{-3} mm μA^{-1} cm^{-1} y^{-1}), i_{corr} is the corrosion current density (μA cm^2), $E.W.$ is the equivalent weight (g) and ρ is the density (g cm^{-3}). Using the equivalent weight ($E.W.$ = 12.16 g) and density (ρ = 1.74 g cm^{-3}) (Langford & Wilson, 1978), equation 3 can be reduced to

$$CR(mpy) = 0.90 \, i_{corr} \tag{4}$$

Where i_{corr} is determined for each experiment using Tafel plots. Briefly, a graph is plotted between; electrode potential vs. SCE (Saturated Calomel Electrode) (along Y-axis) and log$i$ (along X-axis). The slopes of tangents to anodic (β_a) and cathodic (β_c) branches are interpolated and their intersection point determines the value of i_{corr} and E_{corr} in the plane of a graph (For more detail, see (Baboian, 2005)).

3

3. Results and Discussion
3.1. XRD Analysis

XRD analysis of Mg-alloy provides information about phases of crystalline structure. Figure 1 shows a variation in the structure before and after carbon implantation. Three main peaks of the untreated alloy have appeared at 32.453°, 34.647°, 36.336°, which are attributed to α- Mg phase as Mg (100), Mg(002) and Mg(101) planes. However, after ion implantation clear variations are observed in these main peaks as well as another phase has been observed. The pure and secondary phase .e., α- Mg and β-Mg$_{17}$Al$_{12}$ are matched very well with the (JCPDS Nos. 04-0770 and 01-1128), respectively. Using Scherrer equation (Langford & Wilson, 1978) and Unit Cell software (Tim Holland and Simon Redfern), crystallites size and lattice parameters of the untreated and treated samples are calculated and given in Table 1:

$$D = \frac{k\lambda}{\frac{\pi}{180}\sqrt{\omega_i^2 - \omega_0^2}\, cos\theta} \tag{5}$$

Where, κ has value 1 and a dimensionless constant that is related to the shape and distribution of crystallites (Klug & Alexander, 1954) λ is the wavelength of X-ray and θ is the Bragg angle. ω_0 and ω_i are the full width at half maximum (FWHM). These results clearly exhibit the effect of carbon ions in the composites of Mg alloys, as the lattice parameters initially decrease and then a slight increment has been observed at the last dose.
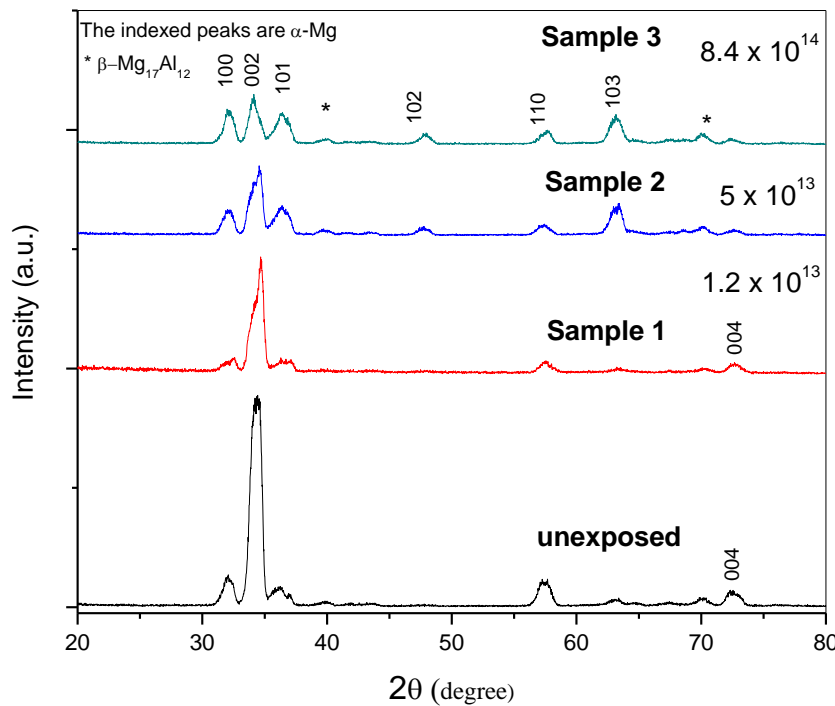
Figure 1: XRD Spectrum of unexposed and exposed AZ91D Mg alloys with variable dose of carbon ion implantation

Table 1
Lattice parameters, cell volume and crystallites size calculated from XRD data

Samples	a (Å)	c (Å)	V (Å)³	D(Å)
Unexposed	3.205	5.186	46.148	276.6
Sample 1	3.194	5.160	45.611	210.1
Sample 2	3.209	5.185	46.244	136.25
Sample 3	3.195	5.269	46.586	175.75

Similarly, crystallite size decreases with the ion implantation, which is also good evidence for the incorporation of carbon ions and a good agreement with the literature (Abdi & Savaloni, 2016). It is revealed that after carbon ion implantation crystallinity decreases with respect to ion dose. The intensity of all the peaks appears suppressed as compared with that of the untreated sample. Moreover, the β-$Mg_{17}Al_{12}$ phase seems to be more prominent for a higher dose of carbon ions, variation in the intensity due to ion implantation has been described by Makinson et al, (Makinson et al., 2000). XRD data reveals that the variation in the intensity, lattice parameters and crystallites play a vital role in the corrosion, which has been discussed in the previous section (B. S. Liu, Wei, Chen, Hou, & Guo, 2015).

3.2. PIXE Analysis

The elemental compositions of; the seawater treated and untreated samples (using PIXE) are shown in Figs. 2(a-b), where the number of counts is plotted against the energy of the emitted characteristic x-rays. Fig. 2(a) depicts the elemental analysis and confirms the existence of Mg, Si, Mn, Al and Zn in AZ91D Mg alloy. It also reveals that after the carbon ion implantation, the peak of Si is suppressed due to the incorporation of C ions. Since carbon and silicon belong to the same group, there is more tendency that the carbon ions may replace the Si position. Due to PIXE limitations of lower atomic number, C ions are not shown in spectra. Whence the variation in peaks predicts the existence of C ions due to the fluence of the ion dose.
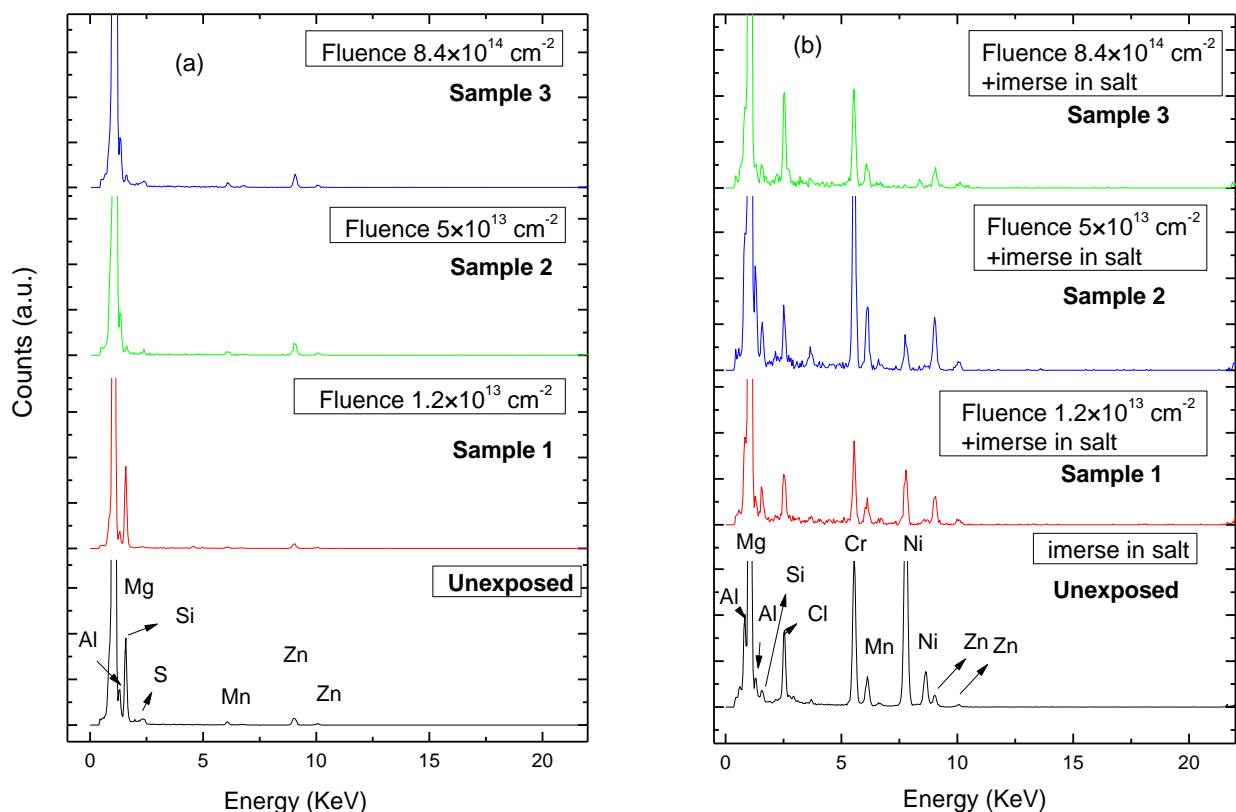

Figure 2: PIXE spectrum of AZ91D Mg alloys; (a) before and (b) after immersion in NaCl with different fluence of C ions

Similarly, Fig 2(b) depicts the elemental analysis of the samples after treated with 3.5 % NaCl solution for 30 days. Results predict a few new elements after immersion in the solution, such as Na, Cl, Ca, Fe, Cr and Ni. Existence of Ni and Cr might be associated with a thick layer of corrosive product, arose on the surface of samples. Although, Cr element is not part of the sample, however, it reacts with the alloy from solution side and becomes

prominent at the surface of the samples, as shown in Fig 2(b). Also, the peak of Ni is due to the reaction of the solution with the sample, as Ni exists in small proportion in AZ91D.

3.3. SEM Analysis

Figure 3 presents the microstructure of AZ91D. The unexposed sample, Fig. 3a (which is alloy matrix) contains large amount α-Mg phase with scattered granular and flower-shaped particles inside the grain and along the grain boundaries. While the images of Carbon implanted ions samples given in Figs. 3(b-d), show micro-cracks on the surface of alloys which may be caused by desorption of water during heat treatment due to incorporation of carbon ions (J. Xu et al., 2017). By increasing, the ion dose from 1.26×10^{13} to 8.4×10^{14} ions-cm^{-2}, the consequent damage also increases, which led to the propagation of microcracks with elongated shape structure to release the accumulated stress (L.-N. Zhang et al., 2013). These irradiation outcomes also guide us for the formation of barrier layers on the surface of specimens, causing the resistance to corrosion and will be discussed later (Uglov, Cherenda, Danilyuk, & Rauschenbach, 2000). One can see that with different ion dose, the surfaces of the exposed samples are changed altogether. The SEM micrographs represent the grey and bright regions that lead to different zones on the surface of Mg-alloy, which is in agreement with the previous study (Suresh et al., 2013; R. Xu et al., 2012).
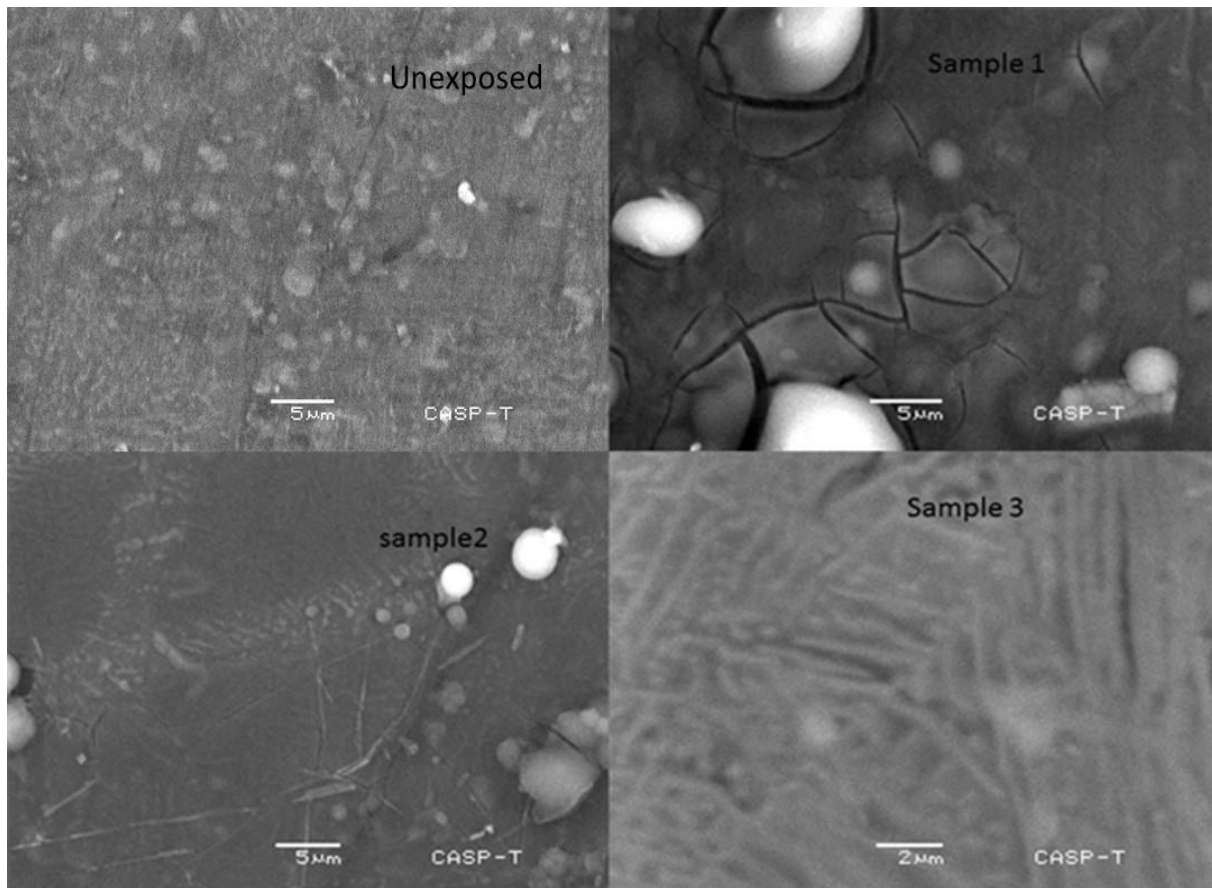

Figure 3: SEM surface images of unexposed sample and samples1, 2, and 3 which exhibit the surface modification due to the appearance of micro-cracks grains and tangled forest of dislocations

3.4. Microhardness Tests

To assess the localized surface modification, the surface morphology of the samples was tested using a Vickers hardness testing instrument. The test was conducted using 200 gm load with a set time of 10 s. Each sample was indented on three neighbouring planar points, thereby calculating the average value of Vickers hardness. The untreated sample stood with HV0 = 82.76. The sample dosed with minimal in the set (1.26×10^{13} ions-cm^{-2}) showed increased hardness HV1 = 83.9, and next higher dosed sample (5×10^{13} ions-cm^{-2})

did not give a remarkable further increase in the hardness HV2 = 84.0 and the highest dosed sample (8.4×10^{14} ions-cm^{-2}) presented the highest value HV3 = 90.1.

The resulting average hardness value was plotted against the corresponding dose as shown in Figure 4. The graph shows that hardness has increased directly with dose. Generally, the measurements and calculations demonstrated that the microhardness tends to increase by increasing dose.
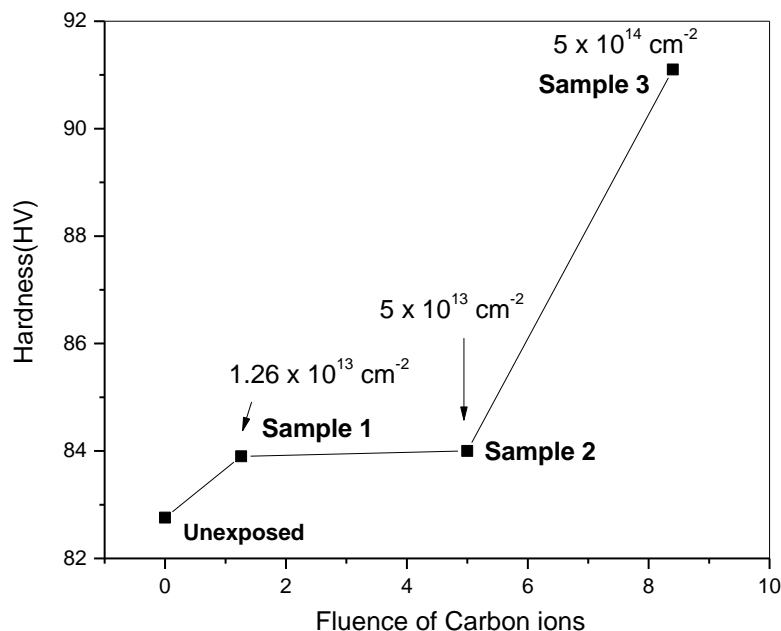
Figure 4: Hardness assessment by using Vickers hardness test against implantation

Microhardness enhancement might be associated with the microstructural defects, the formation of dislocation clusters and re-adjustment of interstitial sites which depends on dislocation density. This, for obvious reasons, has occurred in these samples by C ions implantation. From the microstructural modifications (due to ion dose, as discussed above), the localized increase in hardness can be associated to new phase formations and the distribution of grain size in the matrix, thereby increasing the barrier force. Inferring, these factors may be denounced for the increase in the microhardness which are consequences of ion implantation.

3.5. Corrosion Tests
## 3.5.1. Weight Loss Test

Prepared and treated (carbon ion-implanted) samples of interest were exposed to a corrodent (seawater, 3.5% NaCl solution in this study) for several days to determine the corrosion resistance with the help of loss in mass as given in Table 2. The data are plotted in Figure 5, which shows that there is a trend of reduced mass loss with an increase of ion dose (going from left (non-immersed) to right (more dosed samples)). After 2 days, the loss of mass is the least. Given more immersion time the loss of mass is higher which is an anticipated result. The calculated rate of mass loss is plotted in Figure 6. Results confirm that after thirty days, corrosion resistance and loss in mass are found inversely related. The high dosed sample has maximum corrosion resistance and minimum loss in mass. The results and measurements describe that due to an increase in ion dose of implantation, corrosion resistance also increases the loss of mass of specimens decreases. Which reflects the enhancement effect of corrosion resistance as shown in Figs. 5-6.
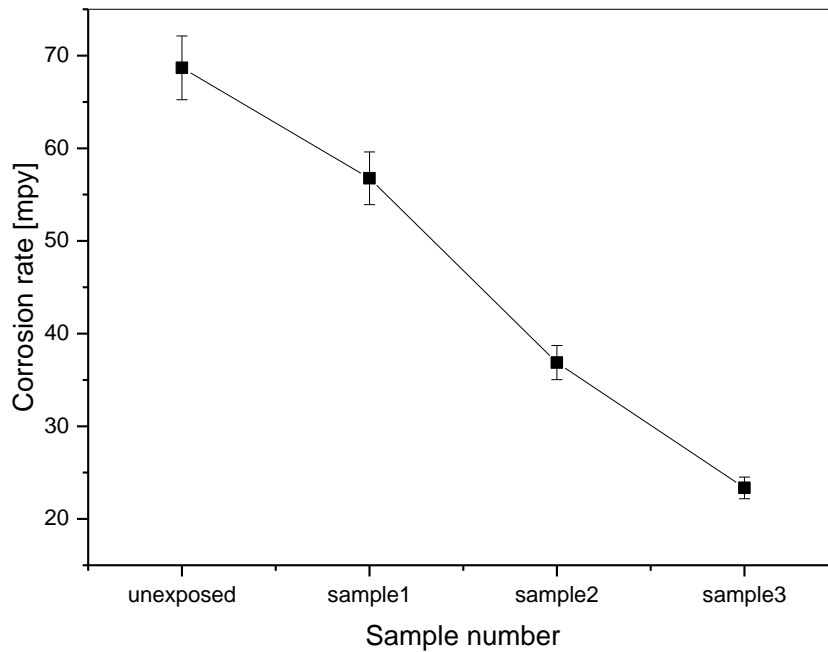
Table 2
Loss in mass of four samples exposed with given doses

Loss of Mass (g)	2 days	10 days	15 days	20 days	30 days

7

|					
Unexposed	0.21	0.54	0.39	0.46	0.66
Sample 1	0.18	0.36	0.34	0.35	0.38
Sample 2	0.12	0.22	0.27	0.26	0.29
Sample 3	0.07	0.18	0.16	0.14	0.12
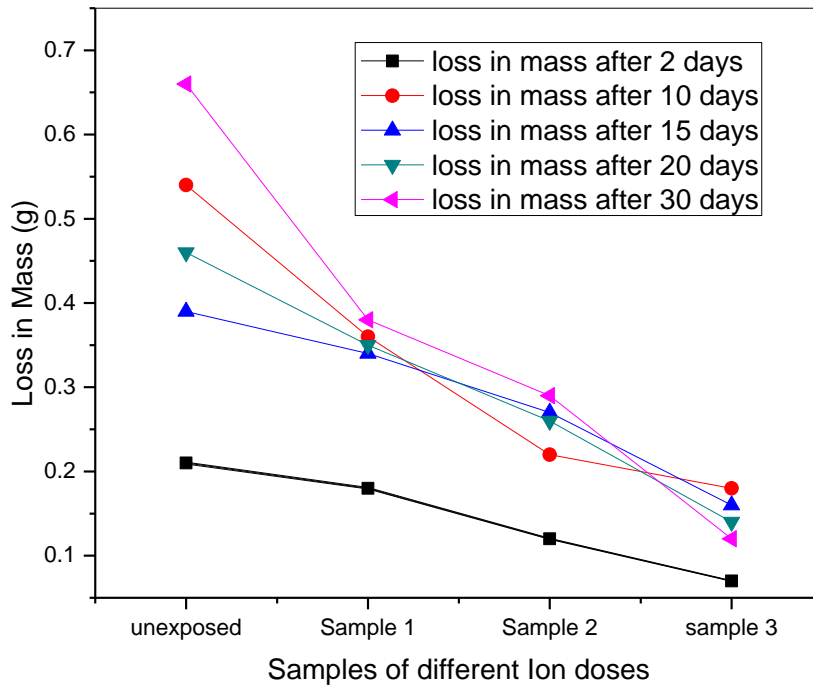
Figure 5: Corrosion resistance increases with increase of ion dose and loss in mass (*W*) decreases

Figure 6: Corrosion rate (mpy) as determined by weight loss method

3.5.2.Electrochemical Test

The electrochemical test results are given in Table 3. The data are plotted in Fig. 7. The trend is obviously the same as of weight-loss method, i.e. the corrosion resistance has increased with ion dose as direct. The tabulated parameters (*Beta A*, *Beta C*, i_{corr} and the *CR*), all have a similar trend of showing values decreasing with dose, but the E_{corr} does not show a similar trend. Which may be associated with the change of mass (loss) due to immersion and the consequent change of shape (corroded) and density of the sample.
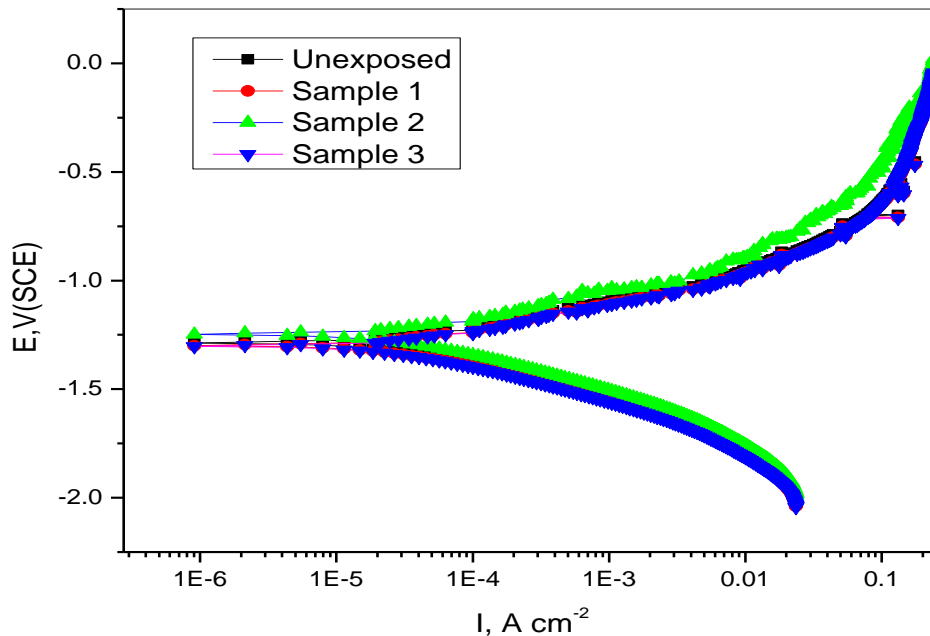
Figure 7: Tafel plots for AZ91D immersed in 3.5 wt. % NaCl solution

Table 3
The electrochemical test parameters and corrosion rate

Electrochemical parameters	Unexposed	Sample1	Sample2	Sample3
Beta A (V/decade)	442.6×10^{-3}	157.5×10^{-3}	129.5×10^{-3}	117.4×10^{-3}
Beta C (V/decade)	344.5×10^{-3}	266.3×10^{-3}	233.7×10^{-3}	188.9×10^{-3}
i_{corr} (µA cm2)	180	112	95.9	67.7
E_{corr} (volts)	-1.37	-1.27	-1.32	-1.35
CR (mpy)	162.4	101	86.5	61.1

It has been observed that the absolute values of corrosion rate just determined should not be considered right away due to various factors not covered in this study. But more important is that the calculated values by using two methods show the same trend of increasing corrosion resistance with dose.

4. Conclusions

Eight samples of AZ91D magnesium alloy were tested, where three pair were implanted with 500 keV energy and a different dose of ions from $1.26 \times 10^{13}, 5 \times 10^{13}$ and 8.4×10^{14} ions-cm^{-2} by using 2 MV Pelletron accelerator. The characterizations of the samples were done by using XRD, SEM, Vickers hardness, weight loss and electrochemical tests for corrosion rate determination. It was found that after carbon ions implantation, the existence of two phases' α-phase and β-phase were confirmed by XRD analysis. Surface modifications and carbon ions interacted structural changes were examined by SEM. From experimental results, we conclude that hardness and corrosion resistance have been progressed. These two effective outcomes have been verified by using a hardness test and corrosion resistance test. Carbon ion implantation on Mg alloy creates productive, astonishing, and effective characteristics at the same time i.e. corrosion resistance and hardness. These two factors play an important and revolutionary role in a variety of applications in preferable, effectual point of view. The improved quality of Mg- alloy may play an impressive role in biocompatibility, aerospace and electromagnetic shielding for

being lightweight and improved characteristics (R. Xu et al., 2014). From the above results of corrosion testing, it can be concluded that carbon-ion implantation on AZ91D Mg-alloy is a useful technique to give strength against corrodents. This ability enhances its commercial exploitation in many aspects (Mao et al., 2015), which works in a way directly related to the ion fluence or the rate of the implantation, which in turn helps improving surface properties.

Acknowledgement

References

Abdi, F., & Savaloni, H. (2016). Influence of N+ ion implantation at different temperatures on nanostructural modifications and characteristics of Al alloy surface. *Philosophical Magazine, 96*(13), 1305-1317. doi:10.1080/14786435.2016.1162912

Baboian, R. (2005). *Corrosion tests and standards: application and interpretation* (Vol. 20): ASTM international.

Butt, M. Z., Ali, D., Aftab, M., Bashir, F., Khalid, M. L., & Khaliq, M. W. (2019). Role of carbon ions implantation in modifying the structural, electrical, and mechanical properties of W–8.57Ni–6.34Cu–1.34Mo alloy. *Physica B: Condensed Matter, 573*, 49-61. doi:https://doi.org/10.1016/j.physb.2019.08.022

Gu, C. D., Yan, W., Zhang, J. L., & Tu, J. P. (2016). Corrosion resistance of AZ31B magnesium alloy with a conversion coating produced from a choline chloride—Urea based deep eutectic solvent. *Corrosion Science, 106*, 108-116. doi:https://doi.org/10.1016/j.corsci.2016.01.030

Höche, D., Blawert, C., Cavellier, M., Busardo, D., & Gloriant, T. (2011). Magnesium nitride phase formation by means of ion beam implantation technique. *Applied Surface Science, 257*(13), 5626-5633. doi:https://doi.org/10.1016/j.apsusc.2011.01.061

Khosro Aghayani, M., & Niroumand, B. (2011). Effects of ultrasonic treatment on microstructure and tensile strength of AZ91 magnesium alloy. *Journal of Alloys and Compounds, 509*(1), 114-122. doi:https://doi.org/10.1016/j.jallcom.2010.08.139

Klug, H., & Alexander, L. (1954). X-ray diffraction procedures, John Willey and Sons. *Inc. New York*, 512.

Langford, J. I., & Wilson, A. (1978). Scherrer after sixty years: a survey and some new results in the determination of crystallite size. *Journal of applied crystallography, 11*(2), 102-113.

Li, P., Han, X. G., Xin, J. P., Zhu, X. P., & Lei, M. K. (2008). Wear and corrosion resistance of AZ31 magnesium alloy irradiated by high-intensity pulsed ion beam. *Nuclear Instruments and Methods in Physics Research Section B: Beam Interactions with Materials and Atoms, 266*(18), 3945-3952. doi:https://doi.org/10.1016/j.nimb.2008.06.030

Li, Y., Lu, F., Li, H., Zhu, W., Pan, H., Tan, G., . . . Ni, G. (2014). Corrosion mechanism of micro-arc oxidation treated biocompatible AZ31 magnesium alloy in simulated body fluid. *Progress in Natural Science: Materials International, 24*(5), 516-522. doi:https://doi.org/10.1016/j.pnsc.2014.08.007

Liu, B. S., Wei, Y. H., Chen, W. Y., Hou, L. F., & Guo, C. L. (2015). Protective compound coating on AZ91D Mg alloy fabricated by combination of cold spraying with die casting. *Surface Engineering, 31*(11), 816-824. doi:10.1179/1743294414Y.0000000439

Liu, H., Xu, Q., Jiang, Y., Wang, C., & Zhang, X. (2013). Corrosion resistance and mechanical property of AZ31 magnesium alloy by N/Ti duplex ion implantation. *Surface and Coatings Technology, 228*, S538-S543. doi:https://doi.org/10.1016/j.surfcoat.2012.04.038

Makinson, J., Lee, J., Magner, S., De Angelis, R., Weins, W., & Hieronymus, A. (2000). X-ray diffraction signatures of defects in nanocrystalline materials. *Adv. X-Ray Anal, 42*, 407-411.

Mao, Y., Li, Z., Feng, K., Guo, X., Zhou, Z., Dong, J., & Wu, Y. (2015). Preparation, characterization and wear behavior of carbon coated magnesium alloy with

electroless plating nickel interlayer. *Applied Surface Science, 327*, 100-106. doi:https://doi.org/10.1016/j.apsusc.2014.11.151

Shafique, M. A., Murtaza, G., Saadat, S., Zaheer, Z., Shahnawaz, M., Uddin, M. K. H., & Ahmad, R. (2016). STUDY OF NICKEL ION RELEASE IN SIMULATED BODY FLUID FROM C+-IMPLANTED NICKEL TITANIUM ALLOY. *Surface Review and Letters, 23*(05), 1650045. doi:10.1142/S0218625X16500451

Song, G., Johannesson, B., Hapugoda, S., & StJohn, D. (2004). Galvanic corrosion of magnesium alloy AZ91D in contact with an aluminium alloy, steel and zinc. *Corrosion Science, 46*(4), 955-977. doi:https://doi.org/10.1016/S0010-938X(03)00190-2

Suresh, M., Srinivasan, A., Pillai, U. T. S., & Pai, B. C. (2013). Mechanism for Grain Refinement and Mechanical Properties of AZ91 Mg Alloy by Carbon Inoculation. *Procedia Engineering, 55*, 93-97. doi:https://doi.org/10.1016/j.proeng.2013.03.225

Tian, X. B., Wei, C. B., Yang, S. Q., Fu, R. K. Y., & Chu, P. K. (2005). Corrosion resistance improvement of magnesium alloy using nitrogen plasma ion implantation. *Surface and Coatings Technology, 198*(1), 454-458. doi:https://doi.org/10.1016/j.surfcoat.2004.10.117

Ueda, M., Reuther, H., & Lepienski, C. M. (2005). Comparison of nitrogen ion beam and plasma immersion implantation in Al5052 alloy. *Nuclear Instruments and Methods in Physics Research Section B: Beam Interactions with Materials and Atoms, 240*(1), 199-203. doi:https://doi.org/10.1016/j.nimb.2005.06.115

Uglov, V. V., Cherenda, N. N., Danilyuk, A. L., & Rauschenbach, B. (2000). Structural and phase composition changes in aluminium induced by carbon implantation. *Surface and Coatings Technology, 128-129*, 358-363. doi:https://doi.org/10.1016/S0257-8972(00)00630-7

Wang, S., Li, C., Xiong, B., Tian, X., & Yang, S. (2011). Surface modification of hard alloy by Y ion implantation under different atmosphere. *Applied Surface Science, 257*(13), 5826-5830. doi:https://doi.org/10.1016/j.apsusc.2011.01.113

Xu, J., Yang, Q., Javed, M. S., Gong, Y., Aslam, M. K., & Chen, C. (2017). The effects of NaF concentration on electrochemical and corrosion behavior of AZ31B magnesium alloy in a composite electrolyte. *RSC advances, 7*(10), 5880-5887.

Xu, R., Yang, X., Li, P., Suen, K. W., Wu, G., & Chu, P. K. (2014). Eelectrochemical properties and corrosion resistance of carbon-ion-implanted magnesium. *Corrosion Science, 82*, 173-179. doi:https://doi.org/10.1016/j.corsci.2014.01.015

Xu, R., Yang, X., Suen, K. W., Wu, G., Li, P., & Chu, P. K. (2012). Improved corrosion resistance on biodegradable magnesium by zinc and aluminum ion implantation. *Applied Surface Science, 263*, 608-612. doi:https://doi.org/10.1016/j.apsusc.2012.09.116

Yan, D., Yu, G., Hu, B., Zhang, J., Song, Z., & Zhang, X. (2015). An innovative procedure of electroless nickel plating in fluoride-free bath used for AZ91D magnesium alloy. *Journal of Alloys and Compounds, 653*, 271-278. doi:https://doi.org/10.1016/j.jallcom.2015.08.210

Zhang, J., Gu, C., Tong, Y., Yan, W., & Tu, J. (2016). A Smart Superhydrophobic Coating on AZ31B Magnesium Alloy with Self-Healing Effect. *Advanced Materials Interfaces, 3*(14), 1500694. doi:https://doi.org/10.1002/admi.201500694

Zhang, J., Gu, C., & Tu, J. (2017). Robust Slippery Coating with Superior Corrosion Resistance and Anti-Icing Performance for AZ31B Mg Alloy Protection. *ACS Applied Materials & Interfaces, 9*(12), 11247-11257. doi:10.1021/acsami.7b00972

Zhang, L.-N., Hou, Z.-T., Ye, X., Xu, Z.-B., Bai, X.-L., & Shang, P. (2013). The effect of selected alloying element additions on properties of Mg-based alloy as bioimplants: A literature review. *Frontiers of Materials Science, 7*(3), 227-236. doi:10.1007/s11706-013-0210-z